Materials Science and Engineering B 304 (2024) 117360

Contents lists available at ScienceDirect

Materials Science & Engineering B

journal homepage: www.elsevier.com/locate/mseb

A novel design and optimization of Si based high performance double absorber heterojunction solar cell

Basra Sultana [a], Md. Ferdous Rahman [b,*], Amaresh Chandra Roy [b], Md. Masum Mia [b], Md. Al Ijajul Islam [b], Ahmad Irfan [c], Aijaz Rasool Chaudhry [d], Md. Dulal Haque [e,*]

[a] Department of Electrical and Electronic Engineering, Southeast University, Dhaka 1208, Bangladesh
[b] Advanced Energy Materials and Solar Cell Research Laboratory, Department of Electrical and Electronic Engineering, Begum Rokeya University, Rangpur 5400, Bangladesh
[c] Department of Chemistry, College of Science, King Khalid University, Abha 61413, P.O. Box 9004, Saudi Arabia
[d] Department of Physics, College of Science, University of Bisha, Bisha 61922, P.O. Box 551, Saudi Arabia
[e] Department of Electronics and Communication Engineering, Hajee Mohammad Danesh Science and Technology University, Dinajpur 5200, Bangladesh

ARTICLE INFO

Keywords:
Silicon
$FeSi_2$
SCAPS-1D
Solar cells
Buffer layer
Efficiency

ABSTRACT

Researchers are currently focusing on Silicon (Si)-based solar cells due to their outstanding semiconductor properties. This study aims to enhance the performance of a new Si based solar cell structure of Cu/FTO/CdS/Si/$FeSi_2$/Au and investigate how the inclusion of $FeSi_2$ as a second absorber and CdS buffer layers affects key performance metrics such as V_{OC}, J_{SC}, FF, and PCE using SCAPS-1D simulation. Various factors including thickness, carrier concentration, defect density, temperature, and electrode design were analyzed in detail to improve performance. The PCE, V_{OC}, J_{SC}, and FF have shown 25.2 %, 0.718 V, 43.3 mA/cm^2, and 80.8 %, respectively with reference structure's (Cu/FTO/CdS/Si/Au). The PCE, V_{OC}, J_{SC}, and FF have improved to 27.73 %, 0.74 V, 45.55 mA/cm^2, and 79.94 %, respectively by adding $FeSi_2$ layer as a bottom absorber with proposed structures (Cu/FTO/CdS/Si/$FeSi_2$/Au). This research has the potential to offer insights and strategies for the development of cost-effective Si-based thin-film solar cells in a near future.

1. Introduction

The development of environmentally friendly and renewable energy sources is a primary goal for scientists and researchers worldwide in an effort to lessen the negative impacts of CO_2 emissions caused by the burning of fossil fuels. Photovoltaic (PV) cells are among the renewable energy sources that are essential for fulfilling the growing demand for energy and advancing green energy [12].The unprecedented mass manufacture of silicon-based solar modules has propelled photovoltaic energy to the forefront as a low-cost, environmentally friendly alternative to traditional electricity generator. At present, silicon dominates the photovoltaic market with a substantial majority share of 90 %. This market is comprised of three unique kinds of silicon: monocrystalline silicon (mono-Si), polycrystalline silicon (poly-Si), and amorphous silicon (a-Si). First generation photovoltaic (PV) technology incorporates both monocrystalline and polycrystalline silicon in its development. Some research has been done in the last few years on monocrystalline silicon solar cells with a thickness of roughly 30 μm using a variety of fabrication techniques in an effort to boost the efficiency of the single-junction cryatalline silicon solar cell with a single bandgap. The effect of varying the thickness of crystalline silicon (c-Si) solar cells from 10 to 80 μm on achieving efficiencies of 15 % to 19 % was investigated by Bozzola et al. [3]. In order to increase the solar cell's optical absorption, M. Hilali et al. [4] used an exfoliation approach to create a c-Si solar cell with a thickness of 25 μm. Theoretical optimization involving the use of a second back reflector layer for a 30 μm thick c-Si solar cell can increase its efficiency by approximately 19.28 % [5].

Amorphous silicon (a-Si:H) thin-film solar cells in particular show promise for cost reduction because of their low material consumption, relatively low production heat requirements, and low temperature coefficient of solar cell performance [6]. However, several third-generation solar cells have been observed to be less efficient and less reliable than commercially available stabilised a-Si:H solar cells [7–11]. At present, the best that a-Si:H solar cells can do in terms of conversion efficiency is 10.2 % [12]. This is still well below the theoretical maximum.

* Corresponding authors.
E-mail addresses: ferdousapee@gmail.com (Md. Ferdous Rahman), dhaque@hstu.ac.bd (Md. Dulal Haque).

https://doi.org/10.1016/j.mseb.2024.117360
Received 10 February 2024; Received in revised form 2 April 2024; Accepted 2 April 2024
Available online 5 April 2024

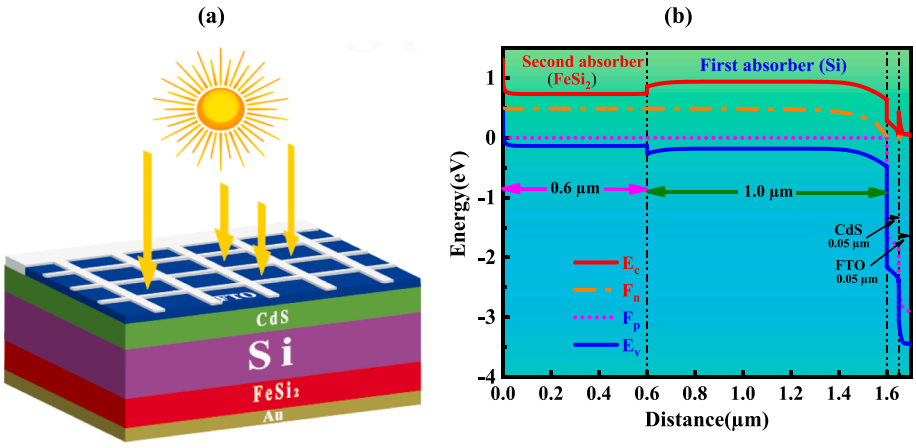

Fig. 1. The Si based proposed new double absorber solar cell (a) device Structure, and (b) energy band diagram.

Silicon clathrates are metastable phases of silicon characterised by their low density. These phases are composed of cage-like frameworks of silicon-atoms, referred to as hosts, which encapsulate atomic or molecule species known as guests [13]. Ongoing research is being conducted in both theoretical and experimental domains pertaining to this particular category of materials. A significant portion of the research efforts have been focused on examining the thermoelectric [14], semiconducting [15,16] and superconducting properties [17–19]. Additionally, optical properties were studied, and they were shown to be promising as photonic materials [20–23]. Several groups [24–27] have recently brought up the possibility of using silicon-clathrates into photovoltaics. The current stage of the fabrication process is in its early phases and is currently being developed with very low efficiency.

To get beyond silicon's shortcomings (its weak absorption coefficience coupled to the indirect bandgap leading to conversion-efficiency constraint), researchers are looking into alternative semiconductor materials. Perovskites are currently the subject of extensive research because of their significant potential as photovoltaic materials, with remarkable conversion efficiency [28]. This is particularly evident in the development of perovskite/tandem solar cells. Despite exhibiting promising features, new semiconductors continue to require expensive, scarce, and occasionally poisonous materials such as cadmium and arsenide.

To improve the low performance, this research utilizes a dual absorber layer comprised of Si and $FeSi_2$ in the FTO/CdS/Si/$FeSi_2$ structure. Research finding [29] highlight that the utilization of two absorber layers in a solar cell results in improved efficiency due to its capacity to absorb solar photons over an extended spectral range. The absorber layer $FeSi_2$ exhibits a direct bandgap energy of 0.87 eV [30] and a significant α value surpassing 10^5 cm^{-1} when exposed to a photon energy of 1 eV [31–33]. Because iron (Fe) and silicon (Si) are abundant in the earth's crust, $FeSi_2$ is an affordable component for solar PV cells' active absorber materials. On the other hand, the $FeSi_2$-based solar cell's competitiveness would be demonstrated by comparing its efficiency to other new technologies, such as perovskite or multi-junction cells, or to conventional structures like single-junction silicon cells[34]. By removing photogenerated electrons from the absorber layer, electron-hole recombination at interfaces is inhibited and hole transmission to the electrode is stopped by ETL. The energy levels of the ETL material must be compatible with the absorber material to harvest electrons and prevent holes. Most commonly, n-type semiconductor materials including ZnS, ZnO, SnO_2, CdS, TiO_2, WO_3, WS_2, PCBM and TMD are considered ETL [35]. Of these, CdS shows great promise as an ETL layer material. Using a CdS electron transport layer, which has high electron mobility, wide bandgap, and low photocatalytic activity, improves SC stability [36].

This study focuses on the examination and improvement of various performance parameters especially V_{OC}, J_{SC}, FF, and PCE with the aim of enhancing the efficiency of silicon based double absorber solar cells. To enhance the efficiency of the SC, several factors such as layer thickness, doping concentration, defect concentration, and interface defect density are examined and adjusted to analyse the output parameters. In addition, the suggested SC's output characteristics and overall adjusted PCE are studied across a range of operating temperatures, series and shunt resistances.

2. Modelling and simulation parameters

The present investigation encompassed the implementation of a computational model on a silicon-based photovoltaic device employing the Solar Capacitance Simulator (SCAPS-1D) software [37]. As a promising tool for building and analysing polycrystalline thin film solar cells (TFSC), the SCAPS program has garnered a lot of attention since its development by the Department of ELIS at the University of Ghent in Belgium. The purpose of the SCAPS-1D models is to simulate light absorption and the formation of electron-hole pairs in the solar cell's active layer. Characteristics such as carrier mobility, carrier lifetime, recombination rates, and bandgap are essential for correctly describing the behavior of the semiconductor material[38]. However, boundary conditions, which include things like temperature, specify the solar cell's operating environment. Changing the doping concentration of the semiconductor material can alter the device's conductivity and recombination rates [39–42]. Additionally, changes in the thickness of various layers-such as the contact, buffer, and absorber layers-have an impact on series resistance, charge carrier collection, and light absorption[43].The fundamental semiconductor equations (equations (1)–(3) are employed in the SCAPS-1D software to describe the system. In SCAPS-1D, the solution of three coupled and nonlinear differential equations is obtained simultaneously [44–48].

$$\frac{\partial^2\psi}{\partial x^2} = -\frac{q}{\varepsilon}\left(p - n + N_D^+ - N_A^- + \frac{\rho_{def}}{q}\right) \tag{1}$$

$$\frac{\partial J_n}{\partial x} - U_n + G = \frac{\partial n}{\partial t} \tag{2}$$

$$\frac{\partial J_p}{\partial x} - U_p + G = \frac{\partial p}{\partial t} \tag{3}$$

The equation denoted as (1) is commonly referred to as the Poisson equation. It is utilized to depict electrostatic phenomena. In this context, ψ represents the electrostatic potential, while n and p correspond to the densities of free electrons and holes, respectively. Additionally, N_D^+ and N_A^- denote the concentrations of ionized donors and acceptors, respectively, while ρ_{def} corresponds to the density of deep defect centers

Table 1
Layer properties of the simulation. [55–61].

Parameters (unit)	FTO	CdS	Si	$FeSi_2$
Thickness(nm)	50	50	1000	600
Bandgap(eV)	3.5	2.4	1.120	0.87
Electron affinity(eV)	4	4.4	4.05	4.16
Dielectric permitivity	9.00	9	11.9	22.6
CB effective DOS(cm^{-3})	1×10^{19}	1.8×10^{19}	2.8×10^{19}	5.6×10^{19}
VB effective DOS(cm^{-3})	1×10^{18}	2.4×10^{18}	1.04×10^{19}	2.04×10^{19}
Electron mobility ($cm^2V^{-1}s^{-1}$)	2.0×10^{1}	100	1500	100
Hole mobility ($cm^2V^{-1}s^{-1}$)	1.0×10^{1}	25	450	25
Donor density N_D (cm^{-3})	1×10^{18}	1×10^{15}	0	0
Acceptor density N_A(cm^{-3})	0	0	1×10^{16}	1×10^{17}
Defect type	Acceptor	Acceptor	Donor	Donor
Bulk defect density,N_t (cm^{-3})	10^{14}	10^{14}	10^{12}	10^{12}
Electron capture cross-section, σe (cm^2)	10^{-15}	10^{-15}	10^{-15}	10^{-15}
Hole capture cross-section, σp (cm^2)	10^{-15}	10^{-15}	10^{-17}	10^{-15}
Defect position above Ev(eV)	0.6	0.6	0.6	0.6

Table 2
Interface parameters used in the BSF/absorber and absorber/ETL interface.

Parameters (unit)	**$FeSi_2$/Si**	**Si/CdS**
Defect type	Neutral	Neutral
Electron capture cross-section, σe (cm^2)	10^{-19}	10^{-19}
Hole capture cross-section, σp (cm^2)	10^{-19}	10^{-19}
Defect position above the highest Ev(eV)	0.6	0.6
Interface Defect density(cm^{-2})	10^{12}	10^{12}

[49–51]. Equations (2) and (3) represent the continuity equations for electrons and holes, respectively. These equations describe the state of dynamic equilibrium within a semiconductor. The variable G denotes the generation rate, while U_n and U_p represent the recombination rates for electrons and holes, respectively. The J_n and J_p are used to denote the current densities associated with electrons and holes, respectively [52–54].

The schematic representation of the device, referred to as FTO/CdS/Si/$FeSi_2$ SC, is illustrated in Fig. 1(a). This design incorporates a p-type material, $FeSi_2$ as the second absorber and employs Si as the first absorber layer. Moreover, the n-type substance CdS serves as the electron transport layer (ETL). Furthermore, the contact material chosen for this study is fluorine doped tin oxide (FTO), whereas the anode material is considered gold (Au). Fig. 1(b) illustrates the energy level diagram of the materials employed in the device architecture. The parameters for the device and the material are broken down and summarized in Tables 1 and 2, respectively.

3. Results and discussion

3.1. Influence of absorber layer thickness and doping density on PV parameter

Fig. 2(a) depicts how the absorber layer's thickness affects the efficiency, fill factor, open circuit voltage and short circuit current density. As the absorber layer thickness increased, a corresponding rise in all solar cell output parameters was observed. At a thickness of 0.3 μm, V_{OC} is found to be 0.701 V and 0.726 V single and double absorber, and it rises to 0.764 V and 0.784 V at 3.0 μm. It was also shown that J_{SC} grew linearly with absorber thickness up to 1.5 μm, after which it essentially plateaued [62].

The observed outcome can be attributed to the significant absorption of incoming photons within the intrinsic layer, leading to an increase in the quantity of photo-generated carriers [10]. Similarly, both FF and efficiency grew with increased thickness. The obtained FF for thicknesses of 0.3 μm and 3.0 μm are 78.36 % and 81.89 %, respectively [63].

The power conversion efficiency is determined at 25.79 % and 28.1 % at 0.3 μm and 3.0 μm thicknesses, respectively. Photovoltaic saturation is seen in Fig. 3 for thicknesses greater than 1.0 μm. For further exploration, the optimal thickness of the Si absorber layer is 1.0 μm.

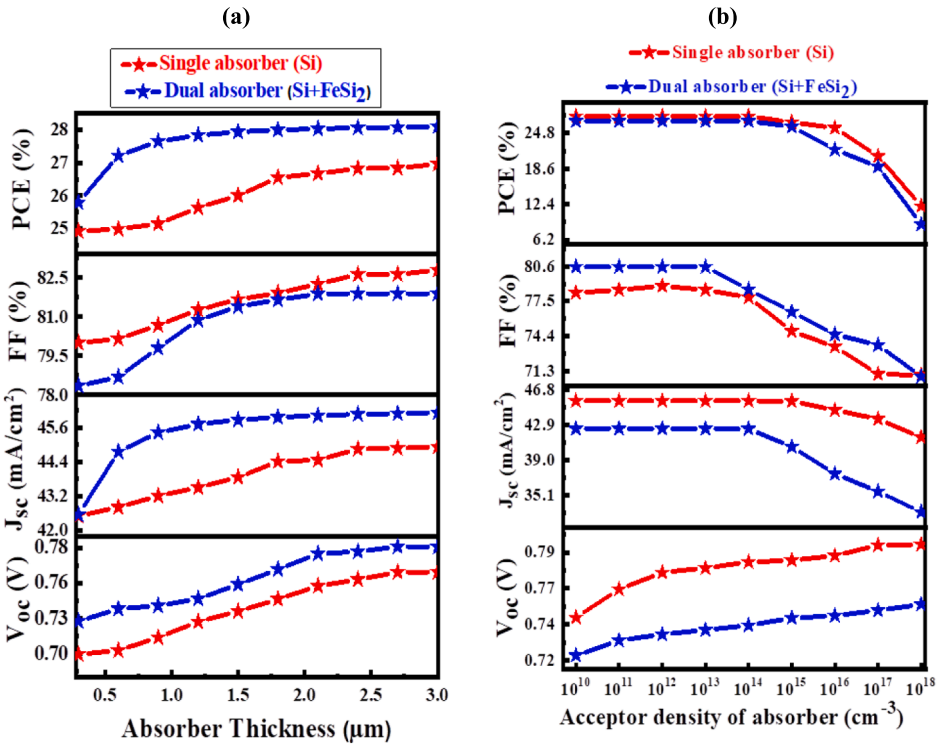

Fig. 2. Impact of variation in (a) absorber layer thickness, and (b) doping density of absorber on PV parameters of V_{oc}, J_{sc}, FF, and PCE.

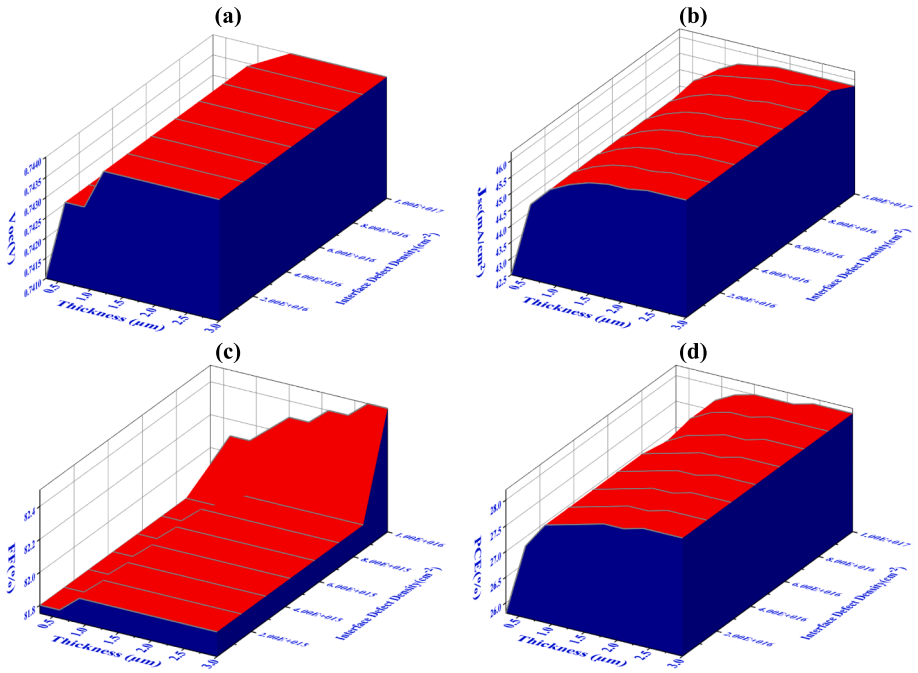

Fig. 3. Impact of thickness and absorber defect density on the photovoltaic performance (a) V_{oc}, (b) J_{sc}, (c) FF, (d) PCE-based on Si absorber solar cell.

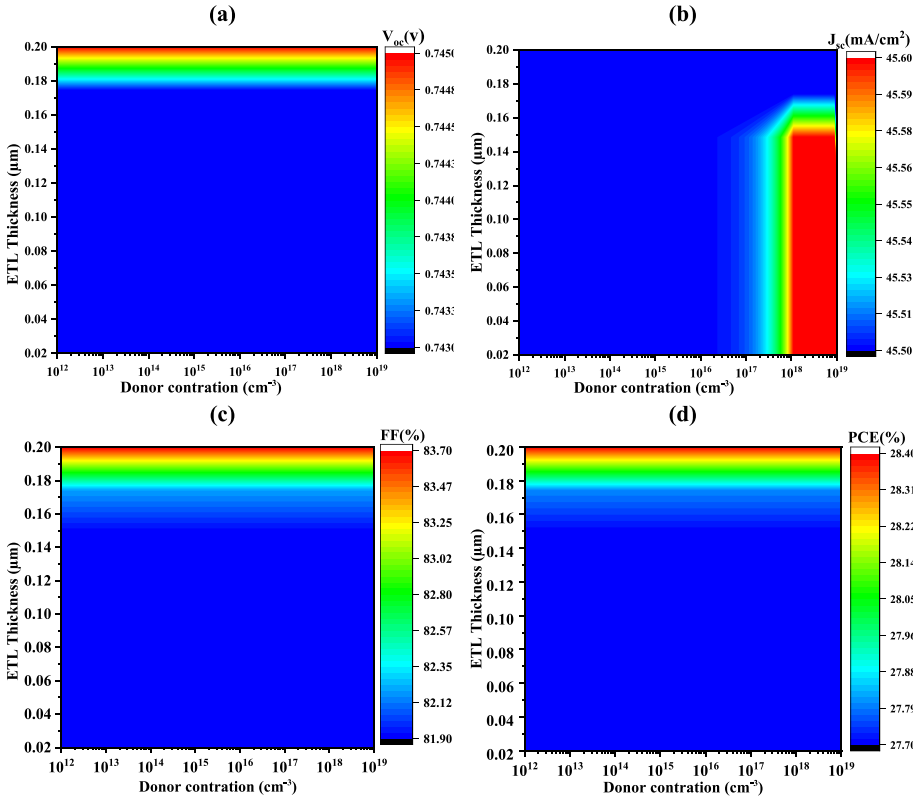

Fig. 4. Impact of thickness and doping concentration of CdS ETL on the photovoltaic performance (a) V_{oc} (b) J_{sc}, (c) FF, and (d) PCE of Si based solar cell.

Fig. 2(b) depicts how the absorber layer's doping concentration affects the solar cell's parameter. Absorber doping density has a nearly insignificant impact on V_{OC}. Both the J_{SC} and FF remain nearly constant up to a doping density of 10^{14} cm^{-3}, beyond which they begin to drop [62,64]. For doping densities up to around 10^{15} cm^{-3}, efficiency is essentially constant; after that, it drops down.

Fig. 3 displays PV characteristics for 0.3 μm to 3 μm absorber thickness and 10^{10} cm^{-3} to 10^{17} cm^{-3} absorber defect density to identify the best absorber thickness and defect density. Both V_{OC} and FF increase absorber thickness up to 1 μm, where they saturate, but they are largely insensitive to changes in defect density [65]. The increase in absorber layer thickness from 0.3 μm to 3.0 μm is associated with a corresponding improvement in efficiency from 25.8 % to 28.1 %.

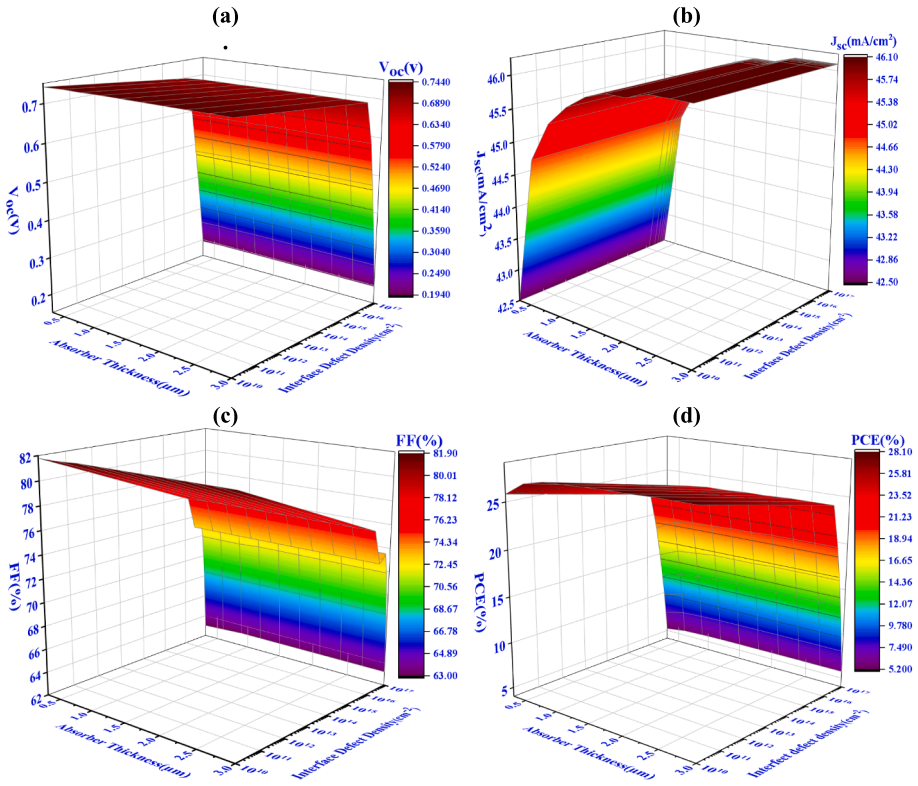

Fig. 5. Effects of absorber thickness and interface defect density (Si/CdS) variations on photovoltaic performance parameters (a) V_{oc} (b) J_{sc} (c) FF and (d) PCE.

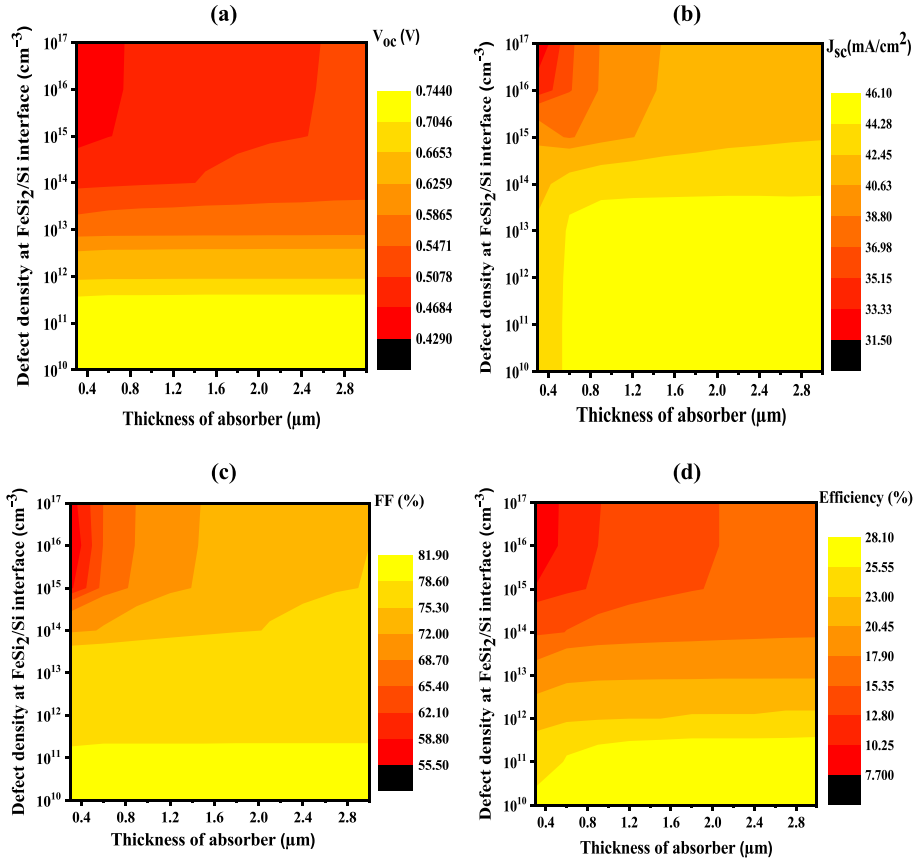

Fig. 6. Effects of absorber thickness and interface defect density ($FeSi_2$/Si) variations on photovoltaic performance parameters (a) V_{oc} (b) J_{sc} (c) FF and (d) PCE.

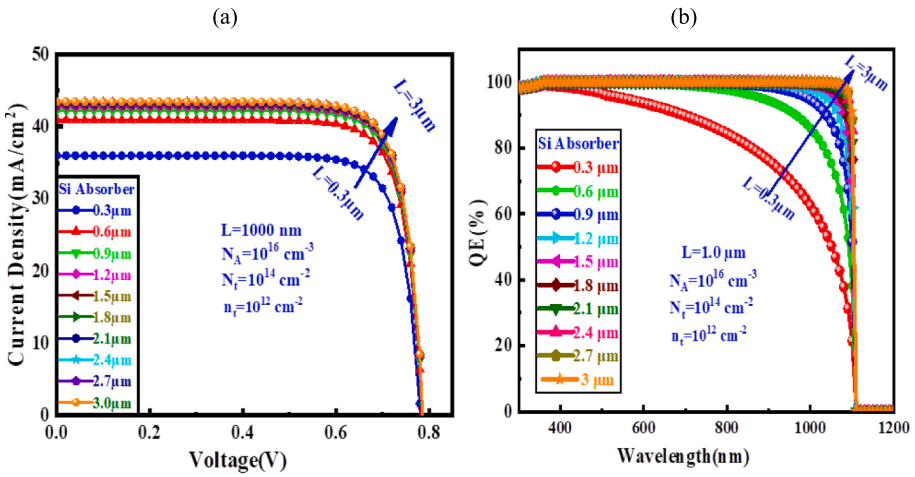

Fig. 7. Impact of the absorber layer thickness of Si solar cell (a) J-V, and (b) QE for various thicknesses.

3.2. *Influence of ETL thickness and doping density on PV parameter*

In Fig. 4, we observe the effects of changing the ETL thickness from 0.02 μm to 0.2 μm and the carrier concentration from 10^{12} cm^{-3} to 10^{19} cm^{-3} on the photovoltaic (PV) properties. The goal of this study is to establish the optimum thickness for the ETL thickness and carrier concentration. Up to 0.16 μm, with a given doping density, the V_{OC}, FF and PCE are nearly constant [59,66], before gradually increasing [67]. When the carrier density is greater than 10^{17} cm^{-3} and the thickness is less than 0.18 μm, the J_{SC} increases. However, the J_{SC} does not change outside of this range. Increased buffer layer doping concentration, generates a strong electric field that efficiently draws electrons and opposes minority carriers away from the ETL/absorber layer interface, thereby decreasing interface recombination [68]. The thickness of 0.05 μm is chosen as optimal in light of all the simulation findings and the cost of production. In this study, a donor density of 1×10^{15} cm^3 for ETL was found to be optimal.

3.3. *Influence of absorber thickness and defect density at Si/CdS interface on PV parameter*

The performance of the suggested solar cell is shown to vary with absorber thickness and defect density at the Si/CdS interface, as shown in Fig. 5. As the interface defect density increases, the V, FF and efficiency all fall for a given absorber thickness [65,67]. The current density, J_{SC} is relatively insensitive to the interface defect density. Fig. 5

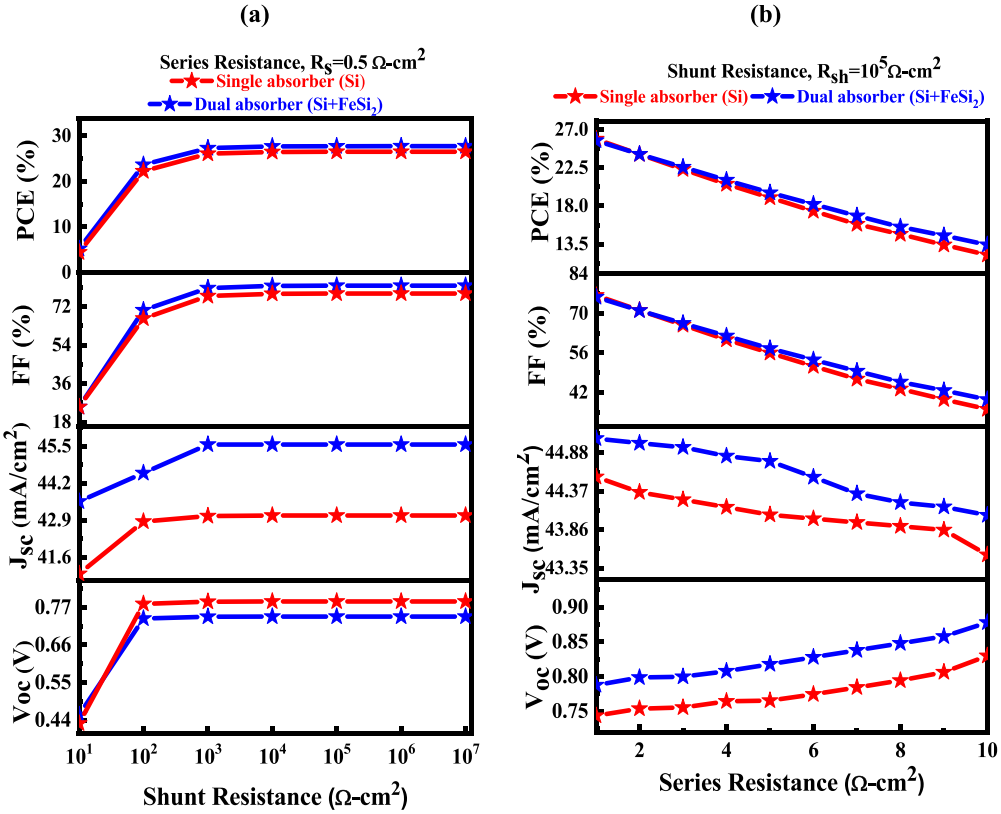

Fig. 8. The impact of varying (a) R_{Sh} and (b) R_S on the characteristics of the proposed Si based solar cell.

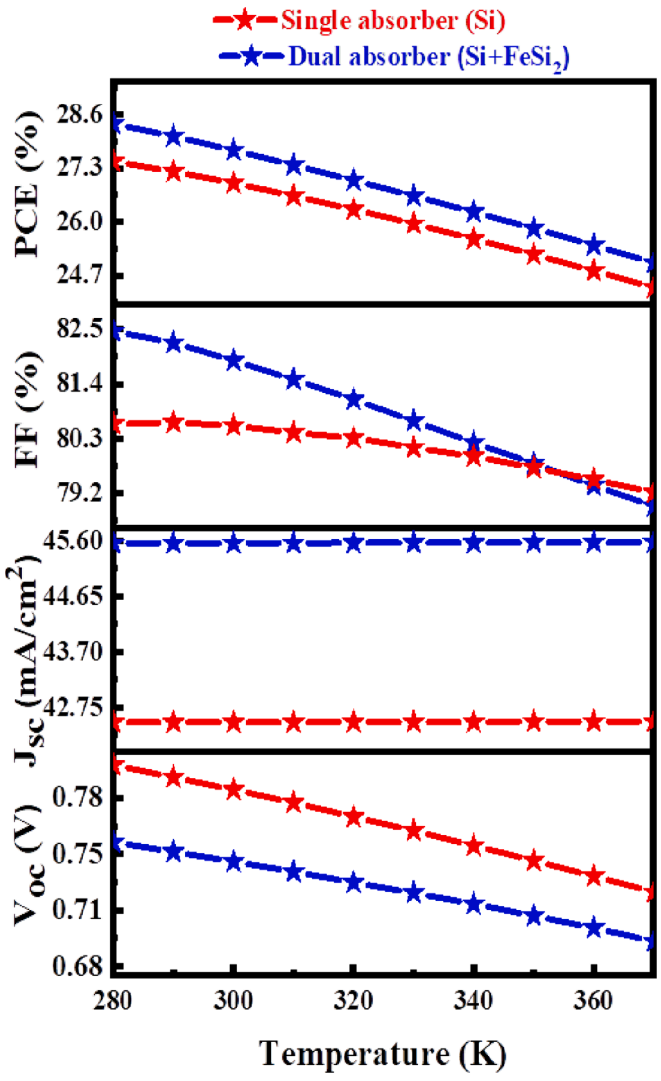

Fig. 9. The temperature effect on the proposed Si based parameters of the cell of the PV.

demonstrates that at a thickness of 1 μm, the V_{OC}, FF and PCE all significantly decrease from 0.744 V to 0.197 V, 81.9 % to 63.4 % and 27.8 % to 5.7 % respectively, as the defect density grows from 1×10^{10} cm^{-3} to 1×10^{17} cm^{-3},. The decrease in efficiency can be attributed to the increase in recombination centers at the interface Si/CdS [69]. Additionally, the presence of electron traps contributes to this phenomenon. Furthermore, optical absorption also influences the observed decline in efficiency. At a certain defect density, the J_{SC} is found to grow proportionally with the thickness of the absorber material.

3.4. *Influence of absorber thickness and defect density at $FeSi_2$/Si interface on PV parameter*

Fig. 6 shows how the performance of the proposed solar cell changes depending on the absorber thickness and the defect density at the $FeSi_2$/Si interface. Photovoltaic characteristics decrease for a given absorber thickness as the interface defect density rises. At an absorber thickness of 1 μm, Fig. 6 shows that as the defect density grows from 1×10^{10} cm^{-3} to 1×10^{17} cm^{-3}, the V_{OC}, J_{SC}, FF and PCE all substantially fall from 0.74 V to 0.43 V, 45.7 mA/cm^2 to 40 mA/cm^2, 81.9 % to 72.1 % and 27.8 % to 13.7 %, respectively [70]. The presence of a high concentration of defects at the $FeSi_2$/Si interface results in the generation of a significant number of hole trap centers, leading to a decrease in the efficiency of the cell [69,71–73]. Taking into account the practical fabrication conditions and stable defect density range at the interface, a defect density of 1×10^{12} cm^{-3} was selected for the suggested SC.

3.5. *Influence of thickness and doping density of absorber on current density and quantum efficiency*

Fig. 7(a) and (c) show the J-V characteristics of optimized solar cell structure with the variation of thickness and carrier concentration of absorber respectively. Both the absorber's thickness and the concentration of its carriers have minimal effects on the current density. Fig. 7 (b) and (d) show how the QE of the SC changes from 300 nm to 1200 nm, depending on the absorber layer thickness and carrier concentration. Over the shorter wavelength range, the QE approaches 100 % before gradually decreasing. Reduced QE is observed at 500 nm for a thickness of 0.3 μm, and at 1050 nm for a thickness of 3 μm as shown in Fig. 7(b) [61,67] As may be seen in Fig. 7(d), the sandwiching of the BSF layer improves the absorption of incident solar spectra, most noticeably between 900 nm and 1100 nm. The enhancement of absorption and the suppression of surface recombination at the FeSi2/Si interface are responsible for the enhancement of the SC's J_{SC} and PCE, which is why the QE is observed to extend at longer wavelengths.

3.6. *Influence of series and shunt resistance on PV parameter*

PV parameter fluctuation at different series and shunt resistances is shown in Fig. 8. The effect of R_{sh} (10^1 Ω–cm^2–10^7 Ω–cm^2) on PV characteristics was examined at a fixed R_s of 0.5 Ω–cm^2 as shown in Fig. 8(a). Up to 10^3 Ω–cm^2, PV parameters vary with R_{sh}, but afterwards they reach a plateau. Previous reports [74] corroborate this effect of R_{sh}. Fig. 8(b) illustrates R_s increases from 1 Ω–cm^2–10 Ω–cm^2 at a fixed R_{sh} of 10^5 Ω–cm^2. When the series resistance increases from 1 Ω–cm^2–10 Ω–cm^2, we observed that the J_{SC}, FF and PCE drops from 44.56 mA/cm^2 to 43.53 mA/cm^2, 76.38 % to 36.11 % and 25.88 % to 12.23 % respectively, while V_{OC} increases from 0.74 V to 0.83 V. Photo-generated carriers recombined severely after generation at high R_s, affecting solar cell performance [75,76].

3.7. *Influence of temperature on PV parameter of proposed Si based double absorber based solar cell*

Fig. 9 illustrates the fluctuations in photovoltaic (PV) characteristics throughout the temperature range of 280 K-370 K. The fill factor (FF) exhibited a decline from 82.46 % to 78.93 %, while the open circuit voltage (V_{OC}) decreased from 0.75 V to 0.69 V. As a result the PCE also decreased from 28.37 % to 25.01 % when the working temperature was increased from 280 K to 370 K [61,77]. The properties of solar cells are significantly influenced by temperature due to the temperature dependent nature of factors such as V_{OC}, J_{SC}, FF and PCE. The temperature-dependent drop in V_{OC} is proportional to the leakage current, J_o which is a measure of the minority carriers across the p-n junction that are thermally generated while the solar cell is in its reverse bias state. An increase in temperature changes the diffusion length and raises stress and strain in the absorber layer, causing deformation and disorder in the layer [78]. These factors ultimately lower the device's overall performance by affecting how well solar cell use sunlight. However, the J_{SC} remains unaffected across the whole temperature range [70]. The proposed solar cell structure demonstrates a commendable thermal response, as evidence by a 3.36 % decrease in PCE within the temperature range of 280 K to 370 K. Temperature increases can cause a drop in photo-conversion efficiency [79] by lowering the band gap of Si and increasing the collision between vibration atoms and photo-generated carriers.

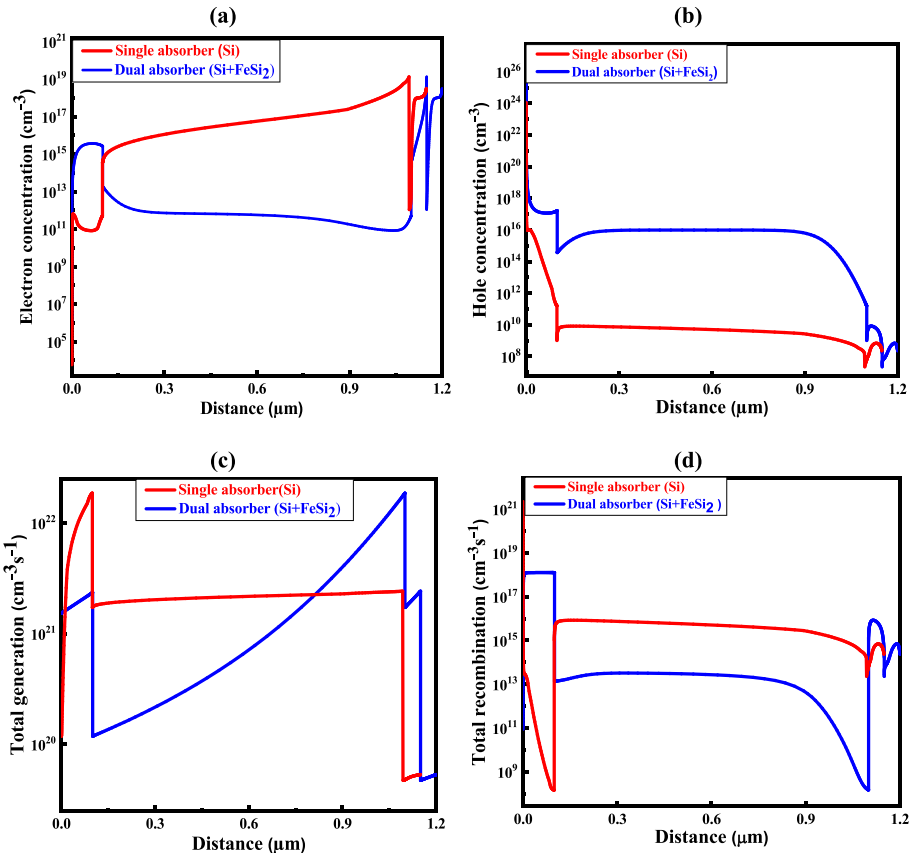

Fig. 10. Influence of (a) electron, (b) hole carrier concentration, (c) total generation, and (d) total recombination concerning the absorber layer thicknesses.

Table 3
A comparative study of the performance of Si-based solar cells.

Research type/ parameters	Device Structure	J_{SC} (mA/ cm^2)	V_{OC} (V)	FF (%)	PCE (%)	Ref.
Experimental	p-(a-SiO_x)/ buffer layer/i-(a-Si: H)/n-(a-Si:H)/ ITO/Al	17.2	0.87	70	10.58	[65]
	p-Si/n-Si/ n^{++}Si	37.7	0.62	78	18.9	[87]
Simulation	p-(a-SiO_x)/ buffer layer/i-(a-Si: H)/n-(a-Si:H)/ ITO/Al	18.95	0.973	68.86	12.71	[65]
	n-Si/p-Si/ p^{++}Si	19.34	0.699	83.48	11.93	[88]
	CZTS/Si based solar cell	19.38	1.4	83.5	22.9	[88]
	CIGS/Si based solar cell	15.8	1.25	81.5	19.8	[89]
	c-Si/SiGe based solar cell	30.25	1.018	80.35	24.74	[55]
	p-Si/n-Si/ n^{++}Si	16.09	0.66	81.3	15.56	[90]
	a-Si/FeSi2/Si	13.31	1.982	0.762	19.80	[91]
	Perovskite/ Silicon Tandem cell	16.01	1.76	86.7	24.4	[90]
	Cu/FTO/CdS/ Si/$FeSi_2$/Au	45.55	0.74	79.94	27.73	This work

3.8. Effect of the carrier concentration of the absorber layer on the G-R profile

The overall generation-recombination (G-R) profiles and carrier (electron and hole) concentration as a function of absorber layer thickness with single and double absorber are shown in Fig. 10. When a double absorber is present, it is evident that the electron concentration of the absorber is reduced compared to the single absorber. The absorber hole concentration, on the other hand, is increased in the presence of a double absorber relative to single absorber. The carrier generation and recombination profiles produced by a systematic investigation showed the potential of the SC with single and dual absorber when compared to other studies at a given and regulated carrier concentration and defect density [80–84].

Photo-generation refers to the phenomenon in which electrons acquire energy and transition from the valence band to the conduction band. Recombination, on the other hand, can be defined as the process in which electrons in the conduction band lose energy and return to the energy state of a hole in the valence band [85]. The rate of photo-generation plays a crucial role in the functioning of solar cells. The number of electrons created at each location in the device owing to photon absorption is represented by the generation rate. Carrier concentrations in the vicinity of a surface are low due to the high recombination rate. The total performance of a solar cell can be improved if the rate of carrier creation is larger than the rate of carrier recombination [86]. According to the findings of the simulation, the rate of photo-generation is greater than the rate of recombination.

Table 3 presents a comparative analysis of the progress made in the investigation of solar cell structures based on Si by various research groups. The prior analysis shows efficiency rising from 10.58 % to 24.74 %. Our study found improved V_{OC}, J_{SC}, FF and PCE compared to earlier research. This study offers new design principles for optimizing Si-based

solar cells with a $FeSi_2$ second absorber layer for 27.73 % efficiency. By coupling a second absorber layer ($FeSi_2$), the voltage, current and PCE can be greatly increased while the absorbers thickness is greatly decreased. Table 3 demonstrates that the TFSC proposed here, even with a thin 1.6 μm (Si + $FeSi_2$) absorber layer, may offer greater economic flexibility than the other Si-based design solar cells displayed in Table 3. The configuration also provides an opportunity to reduce the cost of the absorber material used in (Si + $FeSi_2$) based solar cells. As a result, the proposed solar cell has greater efficiency than its Si and $FeSi_2$ based solar cells.

4. Conclusions

This paper presents an analysis of the photovoltaic (PV) performance of new Si-based solar cells, conducted through numerical investigation using the SCAPS-1D solar simulator with a $FeSi_2$ layer serving as the bottom absorber. The study explores how various device characteristics influence the outputs of solar cells. Optimal parameters, including a Si absorption layer thickness of 1 μm and doping density of (1×10^{16} cm^{-3}), as well as a CdS ETL thickness of 0.05 μm and doping density of (1×10^{15} cm^{-3}), were determined to achieve a high PCE for the proposed structure. It was discovered that a defect concentration of 1×10^{12} cm^{-3} for $FeSi_2$/Si and Si/CdS was optimal at the contact interface. The newly proposed Si hetero-structure incorporating $FeSi_2$ as a bottom absorber demonstrated superior PV characteristics compared to the reference solar cell, with a PCE of 27.73 %, V_{OC} of 0.74 V, J_{SC} of 45.55 mA/cm^2, and FF of 79.94 %. The inclusion of $FeSi_2$ as a second absorber in the suggested solar cell aims to enhance thermal stability for PV performance parameters at high temperatures. The Cu/FTO/CdS/Si/$FeSi_2$/Au structure shows potential for integration into solar cells to improve efficiency.

CRediT authorship contribution statement

Basra Sultana: . **Md. Ferdous Rahman:** Writing – review & editing, Writing – original draft, Visualization, Validation, Supervision, Software, Resources, Methodology, Investigation, Formal analysis, Data curation, Conceptualization. **Amaresh Chandra Roy:** Writing – review & editing, Writing – original draft, Visualization. **Md Masum Mia:** Writing – review & editing, Writing – original draft, Visualization. **Md. Al Ijajul Islam:** Writing – review & editing, Writing – original draft. **Ahmad Irfan:** Writing – review & editing, Writing – original draft, Visualization. **Aijaz Rasool Chaudhry:** Writing – review & editing, Writing – original draft, Visualization. **Md. Dulal Haque:** Writing – review & editing, Writing – original draft, Visualization.

Declaration of competing interest

The authors declare that they have no known competing financial interests or personal relationships that could have appeared to influence the work reported in this paper.

Data availability

Data will be made available on request.

Acknowledgments

A. Irfan extends his appreciation to the Deanship of Research and graduate studies at King Khalid University for funding this work through Large Groups Research Project under grant number R.G.P.2/156/45. A. R. Chaudhry is thankful to the Deanship of Graduate Studies and Scientific Research at the University of Bisha, for supporting this work through the Fast-Track Research Support Program.

References

[1] L.F. Abdulrazak, A. Islam, M.B. Hossain, Towards energy sustainability: Bangladesh perspectives, Energ. Strat. Rev. 38 (2021) 100738, https://doi.org/10.1016/j.esr.2021.100738.
[2] D. Behera, A. Dixit, A. Azzouz-Rached, A. Bentouaf, M. Ferdous Rahman, H. Albalawi, A. Bouhenna, E.S. Yousef, R. Sharma, Prediction of new MAX phase Zr2MSiC2 (M = ti, V) compounds as a promising candidate for future engineering: DFT calculations, Mater. Sci. Eng. B 301 (2024) 117141, https://doi.org/10.1016/j.mseb.2023.117141.
[3] A. Bozzola, P. Kowalczewski, L.C. Andreani, Towards high efficiency thin-film crystalline silicon solar cells: the roles of light trapping and non-radiative recombinations, J. Appl. Phys. 115 (2014).
[4] M.M. Hilali, S. Saha, E. Onyegam, R. Rao, L. Mathew, S.K. Banerjee, Light trapping in ultrathin 25 μm exfoliated si solar cells, Appl. Opt. 53 (2014) 6140–6147.
[5] A.K. Dikshit, P. Banerjee, N. Mukherjee, P. Chakrabarti, Theoretical optimization of double dielectric back reflector layer for thin c-si based advanced solar cells with notable enhancement in MAPD, Superlattice. Microst. 149 (2021) 106747.
[6] L. Martini, L. Serenelli, F. Menchini, M. Izzi, M. Tucci, Silicon heterojunction solar cells toward higher fill factor, Prog. Photovolt. Res. Appl. 28 (2020) 307–320.
[7] S. Banerjee, S. Mandal, S. Dhar, A.B. Roy, N. Mukherjee, Nanomirror-embedded back reflector layer (BRL) for advanced light management in thin silicon solar cells, Ind. Eng. Chem. Res. 58 (2019) 12678–12686.
[8] S. Sriraman, S. Agarwal, E.S. Aydil, D. Maroudas, Mechanism of hydrogen-induced crystallization of amorphous silicon, Nature 418 (2002) 62–65.
[9] J.-É. Bourée, P.R. i Cabarrocas, Cellules solaires en couches minces à base de silicium, Reflets de La Physique. (2007) 12–15.
[10] M.I. Kabir, S.A. Shahahmadi, V. Lim, S. Zaidi, K. Sopian, N. Amin, Amorphous silicon single-junction thin-film Solar cell exceeding 10 % efficiency by design optimization, Int. J. Photoenergy 2012 (2012) 1–7, https://doi.org/10.1155/2012/460919.
[11] M.K. Hossain, Hydrogenated amorphous silicon-based thin film solar cell: optical, electrical and structural properties, Adv. Mat. Res. 1116 (2015) 59–64.
[12] M. Green, E. Dunlop, J. Hohl-Ebinger, M. Yoshita, N. Kopidakis, X. Hao, Solar cell efficiency tables (version 57), Prog. Photovolt. Res. Appl. 29 (2021) 3–15.
[13] S. Yamanaka, Silicon clathrates and carbon analogs: high pressure synthesis, structure, and superconductivity, Dalton Trans. 39 (2010) 1901–1915.
[14] M. Hassan, S.A. Rouf, A.S. Alofi, Q. Mahmood, A. Ishfaq, M. mana AL-Anazy, A.S. Alshomrany, M. Ferdous Rahman, E. SayedYousef, Impact of terbium (Tb) on ferromagnetism and thermoelectric behaviour of spinels MgTb2(S/Se)4 for spintronic, Mater. Sci. Eng.: B. 300 (2024) 117110. Doi: 10.1016/j.mseb.2023.117110.
[15] M. Imai, A. Sato, H. Udono, Y. Imai, H. Tajima, Semiconducting behavior of type-I si clathrate K 8 ga 8 si 38, Dalton Trans. 40 (2011) 4045–4047.
[16] C.W. Myles, K. Biswas, E. Nenghabi, Rattling "guest" impurities in si and ge clathrate semiconductors, Phys. B Condens. Matter 401 (2007) 695–698.
[17] X. Blase, Superconductivity in doped clathrates, diamond and silicon, C. R. Phys. 12 (2011) 584–590.
[18] D. Connétable, V. Timoshevskii, B. Masenelli, J. Beille, J. Marcus, B. Barbara, A. M. Saitta, G.-M. Rignanese, P. Mélinon, S. Yamanaka, Superconductivity in doped s p 3 semiconductors: the case of the clathrates, Phys. Rev. Lett. 91 (2003) 247001.
[19] S. Yamanaka, E. Enishi, H. Fukuoka, M. Yasukawa, High-pressure synthesis of a new silicon clathrate superconductor, Ba8Si46, Inorg. Chem. 39 (2000) 56–58.
[20] R. Himeno, F. Ohashi, T. Kume, E. Asai, T. Ban, T. Suzuki, T. Iida, H. Habuchi, Y. Tsutsumi, H. Natsuhara, Optical band gap of semiconductive type II si clathrate purified by centrifugation, J. Non Cryst. Solids 358 (2012) 2138–2140.
[21] R. Himeno, T. Kume, F. Ohashi, T. Ban, S. Nonomura, Optical absorption properties of NaxSi136 clathrate studied by diffuse reflection spectroscopy, J. Alloy. Compd. 574 (2013) 398–401.
[22] L.L. Baranowski, L. Krishna, A.D. Martinez, T. Raharjo, V. Stevanović, A. C. Tamboli, E.S. Toberer, Synthesis and optical band gaps of alloyed Si–Ge type II clathrates, J. Mater. Chem. C 2 (2014) 3231–3237.
[23] N.A. Mahammedi, M. Ferhat, T. Tsumuraya, T. Chikyow, Prediction of optically-active transitions in type-VIII guest-free silicon clathrate Si46: a comparative study of its physical properties with type-I counterpart through first-principles, J. Appl. Phys. 122 (2017).
[24] S. Botti, J.A. Flores-Livas, M. Amsler, S. Goedecker, M.A.L. Marques, Low-energy silicon allotropes with strong absorption in the visible for photovoltaic applications, Phys. Rev. B 86 (2012) 121204.
[25] L. Krishna, A.D. Martinez, L.L. Baranowski, N.P. Brawand, C.A. Koh, V. Stevanović, M.T. Lusk, E.S. Toberer, A.C. Tamboli, Group IV clathrates: synthesis, optoelectonic properties, and photovoltaic applications, Physics, Simulation, and Photonic Engineering of Photovoltaic Devices III (8981) (2014) 29–39.
[26] A.D. Martinez, L. Krishna, L.L. Baranowski, M.T. Lusk, E.S. Toberer, A.C. Tamboli, Synthesis of group IV clathrates for photovoltaics, IEEE J. Photovoltaics 3 (2013) 1305–1310.
[27] T. Kume, F. Ohashi, S. Nonomura, Group IV clathrates for photovoltaic applications, Jpn. J. Appl. Phys. 56 (2017) 05DA05.
[28] Y. Wang, P. Gawryszewska-Wilczynsk, X. Zhang, J. Yin, Y. Wen, H. Li, Photovoltaic efficiency enhancement of polycrystalline silicon solar cells by a highly stable luminescent film, Sci. China Mater. 63 (2020) 544–551.
[29] K.K. Mamta, V.N.S. Maurya, Sb2Se3/CZTS dual absorber layer based solar cell with 36.32 % efficiency: a numerical simulation, Journal of Science: Advanced Materials and Devices. 7 (2022) 100445, https://doi.org/10.1016/j.jsamd.2022.100445.

[30] Y. Gao, H.W. Liu, Y. Lin, G. Shao, Computational design of high efficiency FeSi2 thin-film solar cells, Thin Solid Films 519 (2011) 8490–8495.

[31] M. Shaban, A.M. Bayoumi, D. Farouk, M.B. Saleh, T. Yoshitake, Evaluation of photovoltaic properties of nanocrystalline-FeSi2/Si heterojunctions, Solid State Electron. 123 (2016) 111–118.

[32] Y. Saito, H. Katsumata, Structural, Optical and AC Conductivity Studies on Polycrystalline-Si/Nanocrystalline-FeSi2 Composite Thin Films, in: JJAP Conference Proceedings 5th Asia-Pacific Conference on Semiconducting Silicides and Related Materials, 2019 (APAC-Silicide 2019), The Japan Society of Applied Physics, 2020: p. 11301.

[33] G.K. Dalapati, S.L. Liew, A.S.W. Wong, Y. Chai, S.Y. Chiam, D.Z. Chi, Photovoltaic characteristics of p-β-FeSi2 (Al)/n-si (100) heterojunction solar cells and the effects of interfacial engineering, Appl. Phys. Lett. 98 (2011).

[34] M.M.A. Moon, M.H. Ali, M.F. Rahman, J. Hossain, A.B.M. Ismail, Design and simulation of FeSi2-based novel heterojunction Solar cells for Harnessing visible and Near-Infrared light, physica status solidi (a) applications and materials, Science 217 (2020) 1–12, https://doi.org/10.1002/pssa.201900921.

[35] M. Ferdous Rahman, M. Naim Hasan Toki, A. Kuddus, M.K.A. Mohammed, M. Rasidul Islam, S. Bhattarai, J. Madan, R. Pandey, R. Marzouki, M. Jemmali, Boosting efficiency above 30 % of novel inorganic Ba3SbI3 perovskite solar cells with potential ZnS electron transport layer (ETL), Mater. Sci. Eng.: B. 300 (2024) 117073. Doi: 10.1016/j.mseb.2023.117073.

[36] S. Kumar, R. Parthasarathy, A.P. Singh, B. Wickman, M. Thirumal, A.K. Ganguli, Dominant 100 facet selectivity for enhanced photocatalytic activity of NaNbO 3 in NaNbO 3/CdS core/shell heterostructures, catalysis, Sci. Technol. 7 (2017) 481–495.

[37] M. Burgelman, P. Nollet, S. Degrave, Modelling polycrystalline semiconductor solar cells, Thin Solid Films 361–362 (2000) 527–532, https://doi.org/10.1016/S0040-6090(99)00825-1.

[38] A. Laidouci, V.N. Singh, P. Kumar, Heliyon performance evaluation of ZnSnN 2 solar cells with si back surface field using SCAPS-1D : a theoretical study, Heliyon. 9 (2023) e20601.

[39] A. Ait Abdelkadir, M. Sahal, Theoretical development of the CZTS thin-film solar cell by SCAPS-1D software based on experimental work, Mater. Sci. Eng. B 296 (2023) 116710, https://doi.org/10.1016/j.mseb.2023.116710.

[40] V. Deswal, S. Kaushik, R. Kundara, S. Baghel, Numerical simulation of highly efficient Cs2AgInBr 6-based double perovskite solar cell using SCAPS 1-D, Mater. Sci. Eng. B 299 (2024) 117041, https://doi.org/10.1016/j.mseb.2023.117041.

[41] I. Chabri, A. Oubelkacem, Y. Benhouria, A. Kaiba, I. Essaoudi, A. Ainane, Performance optimization of a CsGeI3-based solar device by numerical simulation, Mater. Sci. Eng. B 297 (2023) 116757, https://doi.org/10.1016/j.mseb.2023.116757.

[42] F. Khan, F. Rasheed J., T. Alshahrani, S. Kashif Ali, A.M. Alanazi, A.H. Alsehli, M. M. Alsowayigh, N. Elamin Ahmed, Investigations on performance parameters of graphene interfacial layer modified FASnI3: Zn-based lead-free perovskite solar cells, Mater. Sci. Eng.: B. 301 (2024) 117209. Doi: 10.1016/j.mseb.2024.117209.

[43] Y. Wei, Z. Ma, X. Zhao, J. Yin, Y. Wu, L. Zhang, M. Zhao, Improving the performance of Cu2ZnSn(S, Se)4 thin film solar cells by SCAPS simulation, Mater. Sci. Eng. B 303 (2024) 117296, https://doi.org/10.1016/j.mseb.2024.117296.

[44] S. Ahmmed, A. Aktar, M.F. Rahman, J. Hossain, A.B.M. Ismail, A numerical simulation of high efficiency CdS/CdTe based solar cell using NiO HTL and ZnO TCO, Optik 223 (2020) 165625, https://doi.org/10.1016/j.ijleo.2020.165625.

[45] M.F. Rahman, M.M. Alam Moon, M.K. Hossain, M.H. Ali, M.D. Haque, A. Kuddus, J. Hossain, A.B. Abu, Concurrent investigation of antimony chalcogenide (Sb2Se3 and Sb2S3)-based solar cells with a potential WS2 electron transport layer, Heliyon. 8 (2022) e12034.

[46] J. Al Mahmud, M.F. Rahman, kuddus Abdul, M.H. Ali, M.S. Islam, M.D. Haque, S.R. Al Ahmed, M. Mushtaq, A.B.M. Ismail, Design and Analysis of SnS 2/WS 2/V2O5 Double-Heterojunction Toward High Performance Photovoltaics, Energy Advances. (2023) 19–21. Doi: 10.1039/d3ya00231d.

[47] A. Kuddus, M.K.A. Mohammed, A.K. Al-mousoi, A. Ghosh, S. Bhattarai, R. Pandey, J. Madan, M.K. Hossain, RSC Advances Boosting e ffi ciency above 28 % using e ff ective inorganic perovskite †, (2023) 31330–31345. Doi: 10.1039/D3RA06137J.

[48] M.E. Islam, M.R. Islam, S. Ahmmed, M.K. Hossain, M.F. Rahman, Highly efficient SnS-based inverted planar heterojunction solar cell with ZnO ETL, Phys. Scr. 98 (2023) 1–17, https://doi.org/10.1088/1402-4896/accb13.

[49] M.K. Hossain, D.P. Samajdar, R.C. Das, A.A. Arnab, M.F. Rahman, M.H.K. Rubel, M.R. Islam, H. Bencherif, R. Pandey, J. Madan, M.K.A. Mohammed, Design and simulation of Cs2BiAgI6 double perovskite Solar cells with different electron transport layers for efficiency enhancement, Energy Fuel 37 (2023) 3957–3979, https://doi.org/10.1021/acs.energyfuels.3c00181.

[50] M.K. Hossain, G.F.I. Toki, A. Kuddus, M.K.A. Mohammed, R. Pandey, J. Madan, S. Bhattarai, M.F. Rahman, D.K. Dwivedi, M. Amami, H. Bencherif, D.P. Samajdar, Optimization of the architecture of lead-free CsSnCl3-perovskite solar cells for enhancement of efficiency: a combination of SCAPS-1D and wxAMPS study, Mater. Chem. Phys. 308 (2023) 128281, https://doi.org/10.1016/j.matchemphys.2023.128281.

[51] M.F. Rahman, N. Mahmud, I. Alam, M.H. Ali, M.M.A. Moon, A. Kuddus, G.F.I. Toki, M.H.K. Rubel, M.A. Al Asad, M.K. Hossain, Design and numerical analysis of CIGS-based solar cell with V 2 O 5 as the BSF layer to enhance photovoltaic performance, AIP Adv. 13 (2023) 045309, https://doi.org/10.1063/5.0138354.

[52] M.K. Hossain, S. Bhattarai, A.A. Arnab, M.K.A. Mohammed, R. Pandey, H. Ali, F. Rahman, R. Islam, D.P. Samajdar, J. Madan, H. Bencherif, D.K. Dwivedi, M. Amami, RSC advances Harnessing the potential of CsPbBr 3 -based perovskite solar cells using e ffi cient charge transport materials and global optimization, RSC Adv. 13 (2023) 21044–21062, https://doi.org/10.1039/D3RA02485G.

[53] M.K. Hossain, G.F.I. Toki, I. Alam, R. Pandey, D.P. Samajdar, M.F. Rahman, M. R. Islam, M.H.K. Rubel, H. Bencherif, J. Madan, M.K.A. Mohammed, Numerical simulation and optimization of a CsPbI3-based perovskite solar cell to enhance the power conversion efficiency, New J. Chem. 47 (2023) 4801–4817, https://doi.org/10.1039/d2nj06206b.

[54] M.K. Hossain, G.F.I. Toki, A. Kuddus, M.H.K. Rubel, M.M. Hossain, H. Bencherif, F. Rahman, R. Islam, M. Mushtaq, An extensive study on multiple ETL and HTL layers to design and simulation of high - performance lead - free CsSnCl 3 - based perovskite solar cells, Sci. Rep. (2023) 1–25, https://doi.org/10.1038/s41598-023-28506-2.

[55] T. Shawky, M.H. Aly, M. Fedawy, Performance analysis and simulation of c-Si/SiGe based Solar cell, IEEE Access 9 (2021) 75283–75292, https://doi.org/10.1109/ACCESS.2021.3080391.

[56] J. Hossain, Design and simulation of double-heterojunction solar cells based on si and GaAs wafers, J. Phys. Commun. 5 (2021), https://doi.org/10.1088/2399-6528/ac1bc0.

[57] Y.H. Khattak, F. Baig, S. Ullah, B. Marí, S. Beg, H. Ullah, Numerical modeling baseline for high efficiency (Cu2FeSnS4) CFTS based thin film kesterite solar cell, Optik 164 (2018) 547–555, https://doi.org/10.1016/j.ijleo.2018.03.055.

[58] A. Bala Sairam, Y. Singh, M. Mamta, S. Kumar, V.N.S. Rani, Investigation of different configurations in GeSe Solar cells for their performance improvement, J. Nanomater. (2023), https://doi.org/10.1155/2023/9266072.

[59] M.F. Rahman, M.J.A. Habib, M.H. Ali, M.H.K. Rubel, M.R. Islam, A.B.M. Ismail, M. K. Hossain, Design and numerical investigation of cadmium telluride (CdTe) and iron silicide (FeSi 2) based double absorber solar cells to enhance power conversion efficiency, AIP Adv. 12 (2022) 105317, https://doi.org/10.1063/5.0108459.

[60] R.K. Zahoo, A.N. Saleh, Effect of Carrier concentration and thickness of absorber layer on performance CBTS Solar cell, turkish journal of computer and mathematics, Education 12 (2021) 5056–5064.

[61] M.M.A. Moon, M.H. Ali, M.F. Rahman, J. Hossain, A.B.M. Ismail, Design and simulation of FeSi2-based novel heterojunction Solar cells for Harnessing visible and Near-Infrared light, physica status solidi (a) applications and materials, Science (2020), https://doi.org/10.1002/pssa.201900921.

[62] B.K. Mondal, S.K. Mostaque, J. Hossain, Theoretical insights into a high-efficiency Sb2Se3-based dual-heterojunction solar cell, Heliyon. 8 (2022).

[63] A. El Khalfi, L. Et-taya, Y. Achenani, M. Sahal, L. Elmaimouni, A. Benami, Performance evaluation of Sb2Se3-based solar photovoltaic cells with various ETL and Cu2O as HTL by SCAPS-1D, Karbala Int. J. Mod. Sci. 9 (2023) 3.

[64] R. Kumari, M. Mamta, R. Kumar, Y. Singh, V.N. Singh, 24% efficient, simple ZnSe/Sb2Se3 heterojunction Solar cell: an analysis of PV Characteristics and defects, ACS Omega 8 (2022) 1632–1642.

[65] F.X. Abega, A. Ngoupo, J. Ndjaka, Numerical Design of Ultrathin Hydrogenated Amorphous Silicon-Based Solar Cell, Int. J. Photoenergy 2021 (2021) 1–13, https://doi.org/10.1155/2021/7506837.

[66] M.F. Wahid, M.N. Howlader, N. Ahasan, M.M. Rahman, Performance improvement of CIGS Solar cell: a simulation approach by SCAPS-1D, energy and power, Engineering 15 (2023) 291–306.

[67] M. Hasan Ali, A.T.M. Saiful Islam, M.D. Haque, M. Ferdous Rahman, M. Khalid Hossain, N. Sultana, A.z.m., Touhidul islam, Numerical analysis of FeSi2 based solar cell with PEDOT:PSS hole transport layer, materials today, Communications 34 (2023) 105387, https://doi.org/10.1016/j.mtcomm.2023.105387.

[68] M. Mostefaoui, H. Mazari, S. Khelifi, A. Bouraiou, R. Dabou, Simulation of high efficiency CIGS Solar cells with SCAPS-1D Software, Energy Procedia 74 (2015) 736–744, https://doi.org/10.1016/j.egypro.2015.07.809.

[69] O. Astakhov, V. Smirnov, R. Carius, B.E. Pieters, Y. Petrusenko, V. Borysenko, F. Finger, Relationship between absorber layer defect density and performance of a-si: H and μc-si: H solar cells studied over a wide range of defect densities generated by 2 MeV electron bombardment, Sol. Energy Mater. Sol. Cells 129 (2014) 17–31.

[70] B. Sultana, A.T.M.S. Islam, M.D. Haque, A. Kuddus, M.H. Ali, M.F. Rahman, Numerical study of MoSe2-based dual-heterojunction with In2Te3 BSF layer toward high-efficiency photovoltaics, Phys. Scr. 98 (2023), https://doi.org/10.1088/1402-4896/acee29.

[71] J. Tao, X. Hu, J. Xue, Y. Wang, G. Weng, S. Chen, Z. Zhu, J. Chu, Investigation of electronic transport mechanisms in Sb2Se3 thin-film solar cells, Sol. Energy Mater. Sol. Cells 197 (2019) 1–6, https://doi.org/10.1016/j.solmat.2019.04.003.

[72] Y. Wang, Z. Xia, J. Liang, X. Wang, Y. Liu, C. Liu, S. Zhang, H. Zhou, Towards printed perovskite solar cells with cuprous oxide hole transporting layers: a theoretical design, Semicond. Sci. Technol. 30 (2015) 54004, https://doi.org/10.1088/0268-1242/30/5/054004.

[73] Y. Xiao, H. Wang, H. Kuang, Numerical simulation and performance optimization of Sb2S3 solar cell with a hole transport layer, Opt. Mater. 108 (2020) 110414, https://doi.org/10.1016/j.optmat.2020.110414.

[74] A. Hosen, M.S. Mian, S.R. Al Ahmed, Simulating the performance of a highly efficient CuBi 2 O 4-based thin-film solar cell, SN, Appl. Sci. 3 (2021) 1–13.

[75] G.K. Liyanage, A.B. Phillips, M.J. Heben, Role of band alignment at the transparent front contact/emitter interface in the performance of wide bandgap thin film solar cells, APL Mater. 6 (2018) 101104, https://doi.org/10.1063/1.5051537.

[76] M.M. Khatun, A. Sunny, S.R. Al Ahmed, Numerical investigation on performance improvement of WS2 thin-film solar cell with copper iodide as hole transport layer, Sol. Energy 224 (2021) 956–965, https://doi.org/10.1016/j.solener.2021.06.062.

[77] M.D. Haque, M.H. Ali, A.Z.M.T. Islam, Efficiency enhancement of WSe2 heterojunction solar cell with CuSCN as a hole transport layer: a numerical simulation approach, Sol. Energy 230 (2021) 528–537, https://doi.org/10.1016/j.solener.2021.10.054.

[78] X. Zhang, T. Li, Q. Wei, C. Peng, W. Li, X. Ma, Z. Cheng, J. Wu, J. Su, W. Li, Germanium–lead double absorber layer perovskite solar cells: further performance enhancement from the perspective of device simulation, Opt. Commun. 530 (2023) 129188.
[79] S.R. Al Ahmed, A. Sunny, S. Rahman, Performance enhancement of Sb2Se3 solar cell using a back surface field layer: a numerical simulation approach, Sol. Energy Mater. Sol. Cells 221 (2021) 110919, https://doi.org/10.1016/j.solmat.2020.110919.
[80] Y. Cao, C. Liu, J. Jiang, X. Zhu, J. Zhou, J. Ni, J. Zhang, J. Pang, M.H. Rummeli, W. Zhou, H. Liu, G. Cuniberti, Theoretical insight into high-efficiency triple-junction tandem Solar cells via the band engineering of antimony chalcogenides, Solar RRL. 5 (2021) 2000800, https://doi.org/10.1002/solr.202000800.
[81] A.E. Delahoy, Z. Cheng, K.K. Chin, Carrier collection in thin-film CdTe solar cells: theory and experiment, Proc. 27th EU PVSEC. (2012) 2837–2842.
[82] A.E.H. Benzetta, M. Abderrezek, M.E. Djeghlal, A comparative study on generation and recombination process of kesterite CZTS based thin film solar cells for different designs, Optik 219 (2020) 165300, https://doi.org/10.1016/j.ijleo.2020.165300.
[83] M. Atowar Rahman, Enhancing the photovoltaic performance of cd-free Cu2ZnSnS4 heterojunction solar cells using SnS HTL and TiO2 ETL, Sol. Energy 215 (2021) 64–76, https://doi.org/10.1016/j.solener.2020.12.020.
[84] R. El Otmani, A. El Manouni, A. Al Maggoussi, Numerical simulation of CZTSe based Solar cells using different Back Surface field layers: improvement and Comparison, J. Electron. Mater. 50 (2021), https://doi.org/10.1007/s11664-020-08712-8.
[85] X. Kang, S. Liu, Z. Dai, Y. He, X. Song, Z. Tan, Titanium dioxide: from engineering to applications, Catalysts 9 (2019) 191.
[86] F. Laquai, D. Andrienko, C. Deibel, D. Neher, Charge carrier generation, recombination, and extraction in polymer–fullerene bulk heterojunction organic solar cells, Elementary Processes in Organic Photovoltaics. (2017) 267–291.
[87] C. Schmiga, H. Nagel, J. Schmidt, 19% efficient n-type czochralski silicon solar cells with screen-printed aluminium-alloyed rear emitter, Prog. Photovolt. Res. Appl. 14 (2006) 533–539.
[88] B. Bibi, B. Farhadi, W. ur Rahman, A. Liu, A novel design of CTZS/Si tandem solar cell: a numerical approach, J. Comput. Electron. 20 (2021) 1769–1778.
[89] K. Kim, J. Gwak, S.K. Ahn, Y.-J. Eo, J.H. Park, J.-S. Cho, M.G. Kang, H.-E. Song, J. H. Yun, Simulations of chalcopyrite/c-si tandem cells using SCAPS-1D, Sol. Energy 145 (2017) 52–58.
[90] K. Amri, R. Belghouthi, M. Aillerie, R. Gharbi, Device optimization of a lead-free perovskite/silicon tandem solar cell with 24.4% power conversion efficiency, Energies 14 (2021) 3383.
[91] J.-R. Yuan, H.-L. Shen, L. Zhou, H.-B. Huang, N.-G. Zhou, X.-H. Deng, Q.-M. Yu, β-FeSi2 as the bottom absorber of triple-junction thin-film solar cells: a numerical study, Chin. Phys. B 23 (2014) 38801.